arXiv:1411.3849v1 [quant-ph] 14 Nov 2014

Femtosecond wavepacket interferometry using the rotational dynamics of a trapped cold molecular ion

J. Martin Berglund,[1] Michael Drewsen,[2] and Christiane P. Koch[1,*]

[1] *Theoretische Physik, Universität Kassel, Heinrich-Plett-Str. 40, D-34132 Kassel, Germany*
[2] *Department of Physics and Astronomy, Aarhus University, Ny Munkegade 120, DK-8000 Aarhus, Denmark*

(Dated: November 17, 2014)

A Ramsey-type interferometer is suggested, employing a cold trapped ion and two time-delayed off-resonant femtosecond laser pulses. The laser light couples to the molecular polarization anisotropy, inducing rotational wavepacket dynamics. An interferogram is obtained from the delay dependent populations of the final field-free rotational states. Current experimental capabilities for cooling and preparation of the initial state are found to yield an interferogram visibility of more than 80%. The interferograms can be used to determine the polarizability anisotropy with an accuracy of about ±2%, respectively ±5%, provided the uncertainty in the initial populations and measurement errors are confined to within the same limits.

I. INTRODUCTION

Interference of waves both in the form of light and massive particles, such as electrons, neutrals, and atoms, has proven to be a very sensitive method of measuring physical quantities (See e.g. Ref. [1] and references therein). This includes precise measurements of electromagnetic fields, gyromagnetic constants, gravitational acceleration and rotation relative to an inertial system. When it comes to interference of quantum objects with internal energy structure, the method of Ramsey interferometry, involving two-level objects, has been in particular successful [2]. The accuracy in determining the internal state energies by Ramsey interferometry scales inversely proportional to the square root of the interrogation time. Trapped individual atomic ions, laser cooled or sympathetically cooled, have led to the most precise measurements to date [3]. Such ions, occupying much less than a cubic micron, are ideal for controlled laser excitations, and they can exhibit coherence time in the range of hundreds of seconds [4].

Here a Ramsey-type interferometer using the rotational levels of a trapped and sympathetically cooled MgH^+ molecular ion [5] is presented, as schematically illustrated in Fig. 1. Compared to the standard version employed in atom interferometry [6], the $\pi/2$ pulses are replaced by off-resonant femtosecond laser pulses which couple to the polarizability anisotropy of the molecule and induce rotational wavepacket dynamics. Each field-free eigenstate in the wavepacket acquires a specific phase during free evolution, equivalent to specific optical path lengths acquired in light interferometry. The resulting field-free populations are obtained from rotational state selective photodisociation spectroscopy [7] as a function of pulse delay. Their dependence on the time delay between the pulses defines the interferogram. The visibility of the interferogram depends on the laser pulse parameters and the initial state. In particular, the visibility can be enhanced by varying the intensity of the second pulse.

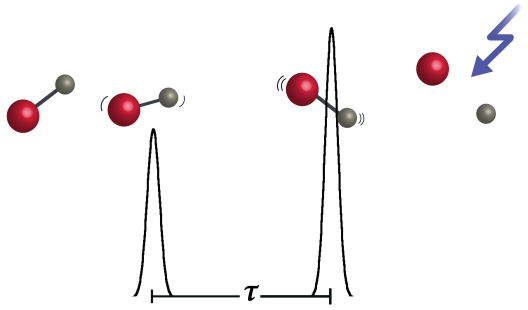

FIG. 1: Schematic illustration of a rotational Ramsey interferometer with time evolving from left to right. A sympathetically cooled MgH^+ molecular ion, initially prepared in its ground state, interacts with a first off-resonant laser pulse (the Mg^+ coolant ion is not shown). Then the resulting wavepacket evolves freely for a controllable time delay τ, until a second pulse is applied, generating a new wavepacket. This step is sensitive to the relative individual phases of the free-field states that make up the wavepacket prior to the second pulse and thus on the time delay. The final rotational populations are measured by a state-sensitive dissociation pulse (blue arrow).

As an application of the interferometer, the measurement of the molecular polarizability anisotropy is discussed, taking both the experimental uncertainties of the initial populations as well as population measurement errors into account. The interferometric method to determine the static dipole polarizabilities discussed here represents, for molecular ions, an interesting alternative to microwave spectroscopy previously used [8, 9]. Conversely, the interferometric technique may be used to probe local electric fields, like the radio-frequency fields at the position of the molecular ion in a (linear) Paul trap. The potentially very long interogation times with trapped ions can make such an interferometer extremely

*Electronic address: E-mail: christiane.koch@uni-kassel.de

sensitive.

The article is organized as follows: Section II introduces the model and numerical tools. The results are presented in Sec. III, starting with an assessment of the effective rotor approximation in Sec. III A, followed by an analysis of the wavepacket created by the first laser pulse and the characterization of the interferograms in Secs. III B and III C. The prospects for measuring the polarizability anisotropy are discussed in Sec. III D. Section IV concludes.

II. THEORETICAL FRAMEWORK

A single trapped MgH^+ ion, translationally cooled down to sub-Kelvin temperatures and in its electronic ground state, is considered. The ion interacts with femtosecond laser pulses which are far off resonance from any transition in MgH^+ and linearly polarized along the laboratory fixed z-axis. The Hamiltonian describing the rovibrational motion of the molecular ion and its interaction with the off-resonant field is given by ($\hbar = 1$)

$$\hat{\mathbf{H}}_{2D} = \hat{\mathbf{T}}_r + V(\hat{\mathbf{r}}) + \frac{\hat{\mathbf{J}}^2}{2m\hat{\mathbf{r}}^2} - \frac{I(t)}{2\epsilon_0 c}\left(\Delta\alpha(\hat{\mathbf{r}})\cos^2\hat{\theta} + \alpha_\perp(\hat{\mathbf{r}})\right), \quad (1)$$

where the first two terms describe the radial kinetic and potential energy, respectively. $\hat{\mathbf{J}}^2$ is the orbital angular momentum operator, and $I(t)$ the intensity profile of the laser pulse. $\Delta\alpha(\hat{\mathbf{r}})$ denotes the molecular polarizability anisotropy and $\alpha_\perp(\hat{\mathbf{r}})$ the molecular polarizability perpendicular to the interatomic axis. θ is the angle between the polarization vector of the laser pulse and the interatomic axis. Assuming linear and parallel pulse polarizations, the Hamiltonian (1) is independent of the azimutal angle ϕ. Therefore $\Delta m = 0$, and the $\cos^2(\theta)$-term gives rise to the selection rule $\Delta j = 0, \pm 2$. The potential curve and polarizabilities are taken from Ref. [10].

In Eq. (1), the leading term of the light-matter interaction is assumed to be via the ion's polarizability anisotropy. The interaction of the light with the permanent dipole moment of the molecular ion has been neglected because it averages to zero if the laser pulses are off-resonant. Simulations of the vibrational dynamics under a pulse with $\lambda_c \approx 800\,\text{nm}$, starting from the ground vibrational level, yield a total population of vibrationally excited levels of the order of 10^{-5} to 10^{-6}, depending on the laser intensity. This confirms that practically no vibrational excitations take place which is not surprising given that the energy difference between the ground and first excited vibrational level corresponds to a wavelength of $\lambda \approx 6500\,\text{nm}$. It is only for $v \approx 10$ that vibrational transitions may become resonant. However, the matrix elements for these transitions is so small that they play essentially no role.

Since for low-lying rovibrational levels the vibrational energy is much larger than the rotational energy, the two degrees of freedom can be adiabatically separated [11].

$B_{\nu=0}$	$\langle\Delta\alpha\rangle_{\nu=0}$	$\langle\alpha_\perp\rangle_{\nu=0}$
$6.3685\,\text{cm}^{-1}$	$3.6634\cdot10^{-25}\,\text{cm}^3$	$7.3268\cdot10^{-25}\,\text{cm}^3$

TABLE I: Parameters of MgH^+, used in Hamiltonian (2).

To this end, the vibrational eigenfunctions are obtained by diagonalizing $\hat{\mathbf{H}}_{vib}$, given by the first two terms in Eq. (1). Denoting radial expectation values by $\langle\cdot\rangle_\nu$ for the νth vibrational level, the vibrational motion can be integrated out in Eq. (1). This yields the so-called Effective Rotor Approximation (ERA) [11] where all $\hat{\mathbf{r}}$-dependent quantities in Eq. (1) are replaced by their expectation values,

$$\hat{\mathbf{H}}_\nu = B_\nu\hat{\mathbf{J}}^2 - \frac{I(t)}{2\epsilon_0 c}\left(\langle\Delta\alpha\rangle_\nu\cos^2\hat{\theta} + \langle\alpha_\perp\rangle_\nu\right), \quad (2)$$

with $B_\nu = \frac{1}{2m}\langle r^{-2}\rangle_\nu$. The ERA neglects ro-vibrational couplings but goes beyond the rigid rotor approximation, since its parameters are obtained by integrating over the vibrational motion instead of just replacing $\hat{\mathbf{r}}$ by the equilibrium distance. The values of the molecular parameters in Eq. (2) for MgH^+, calculated using the *ab initio* data of Ref. [10], are listed in Table I; they are found to be in good agreement with the experimental values of Ref. [12].

The rotational dynamics are characterized by the rotational period, $\tau_{rot} = \hbar/(2B_{\nu=0})$, which amounts to $\tau_{rot} \approx 420\,\text{fs}$ for MgH^+. This short rotational period is a consequence of the large difference in the atomic masses and the small hydrogen mass. Rotational wavepacket revivals occur when the wavepacket returns to its initial state. They can be analysed by the correlation function,

$$C(t) = \langle\chi(0)\,|\,\chi(t)\rangle = \sum_j |c_j|^2 e^{-iE_j t}, \quad (3)$$

where $E_j = j(j+1)B$ is the field-free rotational eigenenergy with corresponding eigenfunction,

$$\chi_j^m(\theta) = \langle\theta|j,m\rangle = P_j^m(\theta). \quad (4)$$

Here, $P_j^m(\theta)$ is the associated Legendre function of degree j and order m. Revivals occur at times T, for which $C(T) = C(0)$. That is, the conditions $2\pi k_j = E_j T$ with k_j integer need to be fulfilled simultaneously for all j which make up the wavepacket $|\chi(t)\rangle$.

The laser pulses $\varepsilon(t)$ which create the wavepackets are assumed to have a Gaussian temporal envelope such that the pulse fluence becomes

$$P(I_0,\tau_I) = \frac{2}{\epsilon_0 c}\sqrt{\frac{\pi}{4\ln 2}}I_0\tau_I. \quad (5)$$

Here I_0 is the maximum pulse intensity and τ_I is the full width at half maximum (FWHM) duration of the intensity profile. In particular, for constant fluence $P = P_0$, the intensity and pulse duration are inversely proportional.

Three different initial states will be considered in the investigations presented below. Ideally for wavepacket interferometry, the molecule is in its ground rotational state ($j = 0$). In an experiment, however, a completely pure initial state cannot be fully realized, but recent experiments with MgH^+ ions trapped in a cryogenic environment have led to a nearly 80% rotational ground state population through helium buffer gas cooling [13]. The ideal initial state is therefore compared to a thermal ensemble with a rotational temperature of 20 K and to an incoherent ensemble prepared in current room-temperature experiments by rotational cooling [14] with the same ground state population ($P_0 \sim 0.38$) as a thermal ensemble at 20 K. An incoherent initial state is described by a density operator, $\hat{\rho}$:

$$\hat{\rho}(t=0) = \sum_{j=0}^{\infty} \sum_{m=-j}^{j} a_j \left|j,m\right\rangle \left\langle j,m\right| . \qquad (6)$$

For a thermal state at temperature T, $a_j = g_j \exp(-\beta E_j)/Z$ with $g_j = 2j+1$, $\beta = 1/k_B T$, and $Z = \sum_j g_j \exp(-\beta E_j)$ the partition function, whereas for the experimentally prepared initial state, the values of a_j are taken from Ref. [14].

Since the timescale of the interferometer is much shorter than any decoherence time, the time evolution is coherent and the density operator at time t is given by

$$\hat{\rho}(t) = \hat{\mathbf{U}}(t)\hat{\rho}(0)\hat{\mathbf{U}}^{\dagger}(t) .$$

Inserting Eq. (6), each m state may be considered separately, reducing the numerical effort in the calculations, since the Hamiltonian conserves m. The time-dependent population of the state j', with all corresponding m-states taken into account, is then obtained as

$$\rho_{j',j'}(t) = \sum_{j=0}^{\infty} a_j \sum_{m=j}^{j} \left| \left\langle j',m\right| \hat{\mathbf{U}}(t) \left|j,m\right\rangle \right|^2 , \qquad (7)$$

i.e., each pure state $|j,m\rangle$ is propagated separately, using a Chebychev propagator, and the resulting population is added up incoherently with its proper weight. The summation over the initially populated values of j in Eq. (7) can be truncated at $j^{ini}_{max} = 6$. The basis set expansion in the Legendre polynomials is found to be converged for $j_{max} = 20$, provided $I_0 \leq 4 \times 10^{13}$ W/cm^2.

III. RESULTS

Before presenting the results obtained with Hamiltonian (2), the accuracy of the ERA is checked in Sec. III A. Then the interferometer is analyzed in a stepwise fashion, starting in Sec. III B with the dependence of the wavepacket, that is created by the first pulse, on pulse intensity and duration. The complete interferometer time evolution is presented in Sec. III C, determining pulse parameters that yield high-visibility interferograms. Prospects for using the interferometer to measure the molecular polarizability are discussed in Sec. III D.

A. Accuracy of the effective rotor approximation

The ERA, Eq. (2), is tested against the full rovibrational dynamics, generated by Hamiltonian (1), considering the interaction with one pulse of 100 fs duration. To this end, the radial coordinate in Eq. (1) is represented on a Fourier grid, and the time-dependent Schrödinger equation with Hamiltonian (1) is solved. The absolute difference in the final-time population is found to be within 0.01 for $j = 0, \ldots, 6$ and intensities $I_0 \leq 1 \times 10^{13}$ W/cm^2. The relative error amounts to less than one percent for j up to $j = 4$ and intensities up to 1×10^{13} W/cm^2. For intensities 1×10^{13} W/cm$^2 \leq I_0 \leq 4 \times 10^{13}$ W/cm^2, the absolute error due to the ERA is within 0.015 for $j = 0, \ldots, 6$, whereas the relative error reaches 10% to 15%. While both absolute and relative errors become larger for higher j states, the ERA is applicable for our purposes since low-lying j states ($j \leq 6$) are most relevant for interferometry and only moderate pulse intensities will be considered to ease experimental feasibility.

B. Creating a rotational wavepacket by a single femtosecond laser pulse

Starting from a pure initial state ($j = 0$, $m = 0$), a femtosecond laser pulse creates a rotational wavepacket which, due to the selection rules, is made up of states $j = 0, 2, 4, \ldots$, all with $m = 0$. Since the laser-molecule interaction is off-resonant and Gaussian pulse envelopes are assumed, the composition of the wavepacket is only determined by the intensity and duration of the pulse. The dependence of the final rotational state populations on pulse intensity and duration is shown in Fig. 2 for $j = 0, 2, 4, 6$. Curves of constant pulse duration (intensity) correspond to horizontal (vertical) cuts in Fig. 2. The black line indicates pulses of $\tau_I = 100$ fs duration. Constant pulse fluences correspond to hyperbolas in the landscape, cf. Eq. (5). Hyperbolas are clearly visible in Fig. 2, indicating that it is the pulse fluence that determines the population transfer. For the pulse parameters corresponding to the upper left part of each panel in Fig. 2, the molecule can approximately be described as a two-level system, consisting of the states $j = 0$ and $j = 2$. This should allow for the closest analogy to a Ramsey interferometer as used with atoms [6]. For short pulses, $\tau_I \lesssim 300$ fs, the final populations show a more complicated behavior, with more states being significantly populated, save for very small I_0. A wide range of pulse parameters gives rise to significant population of $j = 2$, see the lower left corner of Fig. 2 (b). Significant population of the $j = 4$ state is obtained for intensities larger than 0.8×10^{13} W/cm^2 and pulses shorter than 150 fs. However, the $j = 4$ state starts to be populated already at smaller pulse intensities. This inhibits a perfect 50%-50% superposition of the states $j = 0$ and $j = 2$.

In a typical experimental setup, the transform-limited pulse duration is fixed, i.e., to 100 fs, whereas the inten-

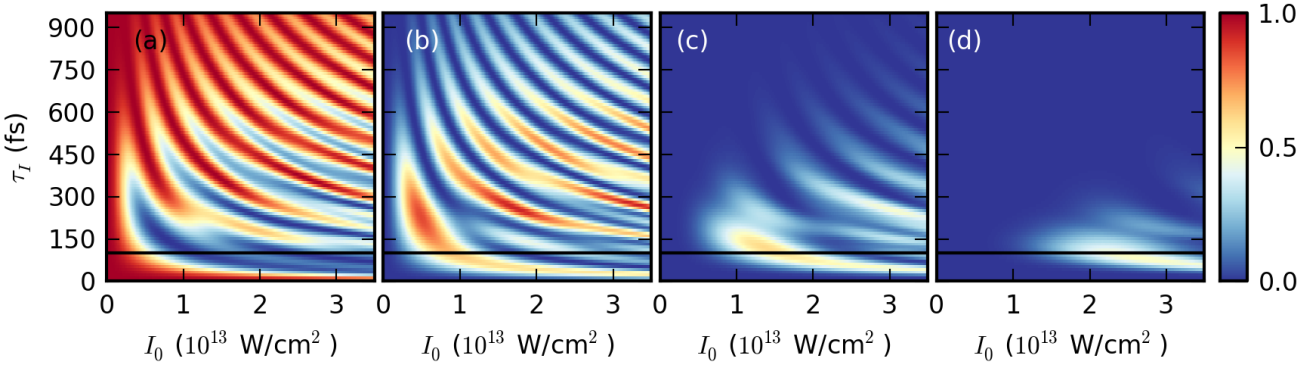

FIG. 2: Final population of field-free rotational states (a: $j = 0$, b: $j = 2$, c: $j = 4$, d: $j = 6$) after interaction with a single laser pulse as function of pulse intensity and duration. The initial state is $j = 0$. The black line indicates pulses of 100 fs FWHM.

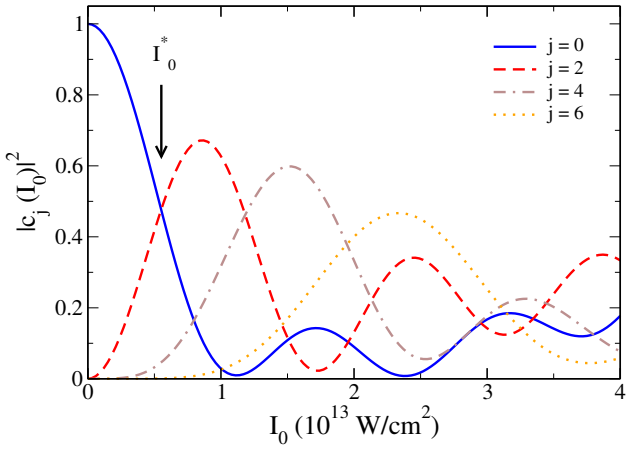

FIG. 3: Final population of field-free rotational states after interaction with a single 100 fs pulse as a function of pulse intensity. The arrow at I_0^* indicates the laser intensity for which equal population of the states $j = 0$ and $j = 2$ is obtained, corresponding to the black line in Fig. 2.

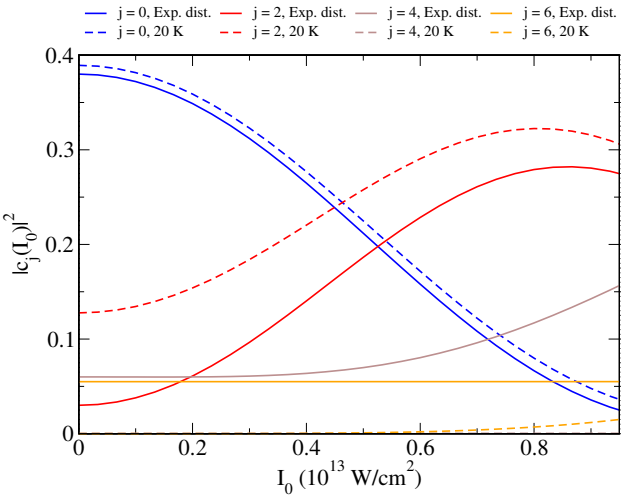

FIG. 4: Same as Fig. 3 but for incoherent initial states, corresponding to the experimental distribution of Ref. [14] (solid lines) and a thermal ensemble at 20 K (dashed lines).

sity is more easily varied. The dependence of the final state populations on pulse intensity for a 100 fs pulse is presented in Fig. 3, as marked by the black lines in Fig. 2. For low intensity, the behaviour is similar to a two-level system, as to be expected from the nearest neighbour coupling in Hamiltonian (2). As the intensity increases, more levels are populated and the result deviates more and more from the simple two-level picture. For even higher pulse intensities, recurring peaks of low j states appear. Note that only a small number of levels can be superimposed at a given field intensity. Intensities for which population curves cross, indicating equal population, are particularly interesting for interferometry since they should yield good contrast. The first such occurrence, at $I_0 \approx 0.5 \cdot 10^{13}$ W/cm^2 for $j = 0$ and $j = 2$, is marked by I_0^* in the figure. Another crossing occurs at $I_0 \approx 1.1 \cdot 10^{13}$ W/cm^2 for $j = 2$ and $j = 4$.

The dynamics becomes more involved for incoherent initial states since in this case also states with $m \neq 0$ are initially populated. Figure 4 shows the final field-free state populations as a function of laser intensity for a 100 fs pulse, comparing two different initial states, the experimental distribution of Ref. [14] and a thermal ensemble at 20 K. The final $j = 0$ population of the two ensembles behaves very similarly, with only a small offset in initial population. Also, both ensembles qualitatively lead to the same dynamics as the pure initial state in Fig. 3, confirming that the ensemble dynamics is dominated by $j = 0$, at least for the intensities examined in Fig. 4. The final $j = 2$ population on the other hand shows some differences between the two initial ensembles, with the peak occurring slightly earlier and the maximum population difference being slightly smaller for the thermal ensemble. For $j = 4$ and $j = 6$, the initial popu-

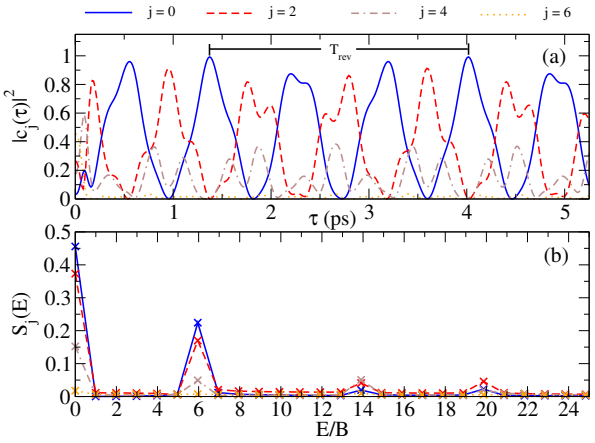

FIG. 5: a: Interferogram, i.e., the final populations of the field-free rotational states, obtained after interaction of the molecule with two laser pulses, as a function of time delay. Both pulses have $I_0 \approx 0.5 \times 10^{13}$ W/cm^2 (as indicated by the arrow in Fig. 3) and $\tau_I = 100$ fs. b: Spectrum S_j of the populations shown in panel (a).

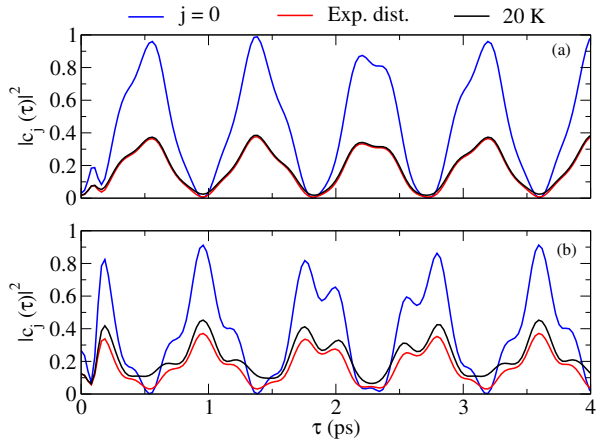

FIG. 6: Interferograms for incoherent initial states, corresponding to the experimental distribution of Ref. [14] (red) and a thermal ensemble at 20 K (black), compared to that of a pure initial state with $j = 0$ (blue): Final populations of the field-free rotational states (a: $j = 0$, b: $j = 2$) as a function of pulse delay. Pulse parameters as in Fig. 5.

lations are negligible in the thermal ensemble and small, but non-zero in the experimental distribution of Ref. [14]. Therefore the resulting final populations after interaction with the pulse in Fig. 4 are similar to those obtained for the pure initial state in Fig. 3. Although the initial population in $j = 4$ and $j = 6$ is non-negligible for the experimental distribution, these states do not take part in the dynamics for pulse intensities up to 0.5×10^{13} W/cm^2. This is promising in view of obtaining high-visibility interferograms even with incoherent initial states.

C. Creating and probing rotational wavepackets using a sequence of two femtosecond laser pulses

Interferograms are obtained when the molecule interacts with two laser pulses, separated by a time delay, τ. For simplicity, the parameters I_0 and τ_I are chosen to be the same for both pulses except where indicated. First, consider the pure initial state with $j = 0$. The laser intensity and pulse duration were chosen such that the first pulse yields equal populations for $j = 0$ and $j = 2$, as marked by I_0^* in Fig. 3. Since very little population is transferred to states other than $j = 0$ and $j = 2$ by the first pulse ($|c_0|^2 = |c_2|^2 \approx 0.47$, $|c_4|^2 \approx 0.06$), a simple interference pattern is obtained in Fig. 5 with the population predominantly in $j = 0$ and $j = 2$ for all time delays. The condition fo revivals of the wavepacket created by the first pulse becomes $T_{rev} = \pi/B \approx 2.6$ ps. The revival time is indicated in Fig. 5, confirming the estimate of 2.6 ps predicted by the correlation function. A very high contrast, or, equivalently, large visibility, is observed for the lower j states. The visibility is defined as

$$V_j = \frac{|c_{j,max}|^2 - |c_{j,min}|^2}{|c_{j,max}|^2 + |c_{j,min}|^2}\,, \tag{8}$$

where $|c_{j,max}|^2$ ($|c_{j,min}|^2$) is the maximum (minimum) population of the jth state. The $j = 0$ state reaches an almost perfect visibility of one and the $j = 2$ state around 0.9, reflecting the almost perfect 50%-50% superposition of these two states.

The Fourier spectra of the delay-dependent final populations in Fig. 5(a) are shown in Fig. 5(b), $S_j = \sqrt{\mathcal{F}[f_j]}$ with $\mathcal{F}$ denoting the Fourier transform and $f_j(\tau) = |c_j(\tau)|^2$. As is evident from Fig. 5(b), the spectrum is useful to visualize the components of the wave packet created by the first pulse, since it displays peaks at the eigenenergies ($E_0 = 0$, $E_2 = 6B$, $E_4 = 20B$) as well as at the quantum beats ($E_{2/4} = 14B$). The similar peak heights of S_0 and S_2 at $E_0 = 0$, $E_2 = 6B$ reflect the almost identical population of the states $j = 0$ and $j = 2$. They differ at higher energies, since population from the $j = 2$ state is further excited into the $j = 4$ state.

Next, Fig. 6 examines the potentially detrimental effect of incoherence in the initial states on the interferogram. It compares the interference patterns for the pure initial state of Fig. 5 with those obtained for the experimental distribution of Ref. [14] and a 20 K thermal ensemble. When measuring the final population of $j = 0$, the two incoherent ensembles give practically identical results, cf. Fig. 6(a). Their delay-dependence is qualitatively the same as that of the pure initial state, but the maximum amplitudes are reduced from close to one down to about 0.4. Notwithstanding, the visibility, V_0, is only reduced to 0.96 for the experimental distribution and 0.91 for the thermal ensemble. For $j = 2$ (Fig. 6(b)), the maximum population still amounts to about 0.4, at least for the

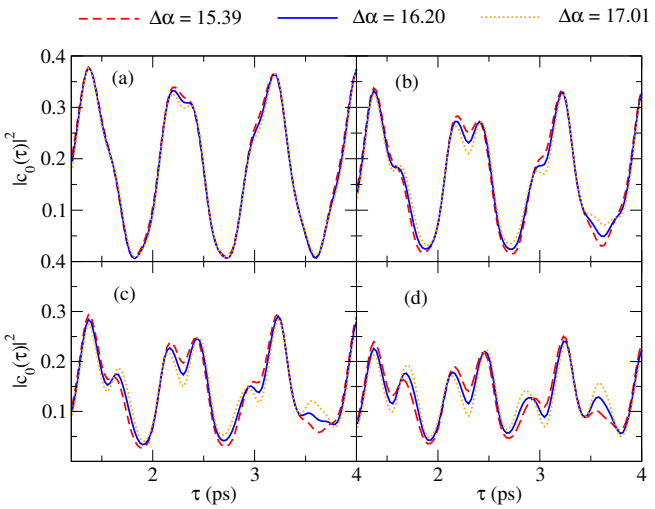

FIG. 7: Interferograms, i.e., final $j = 0$ populations as function of delay, for different values of the polarizability anisotropy $\Delta\alpha$ and increasing intensity of the second pulse (a: identical pulse intensities, b: $I_0^2 = 1.4I_0^1$, c: $I_0^2 = 1.6I_0^1$, d: $I_0^2 = 1.8I_0^1$). The pulse duration is $\tau_I = 100$ fs for both pulses, and the intensity of the first pulse is $I_0^1 = 0.55 \times 10^{13}$ W/cm^2. The initial state corresponds to the experimental distribution of Ref. [14].

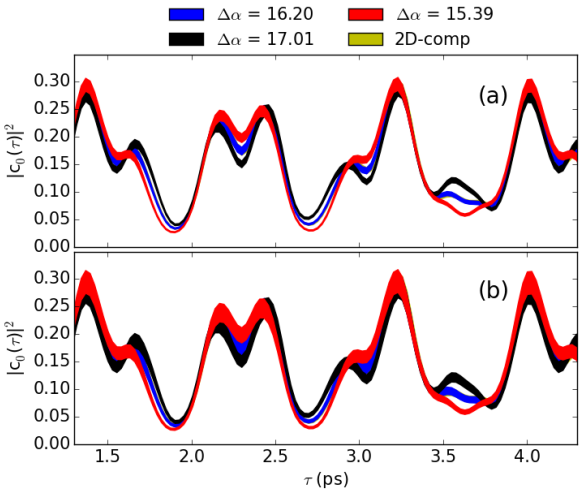

FIG. 8: Interferograms, i.e., final $j = 0$ populations as a function of time delay, for different values of the polarizability anisotropy $\Delta\alpha$, accounting for 2% (a) and 5% (b) measurement uncertainty in the final populations. The initial state corresponds to the experimental distribution of Ref. [14] with 2% uncertainty in the initial populations taken into account ($\tau_I = 100$ fs for both pulses, $I_0 = 0.55 \times 10^{13}$ W/cm^2 for the first pulse, $I_0 = 1.6 \cdot 0.55 \times 10^{13}$ W/cm^2 for the second pulse).

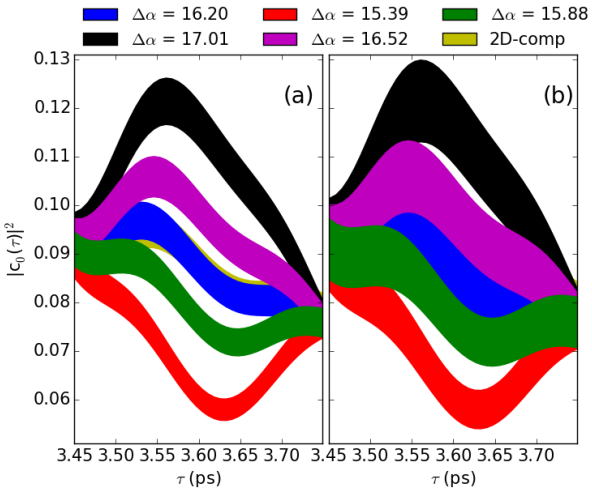

FIG. 9: Same as Fig. 8 for a smaller range of pulse delays, $\tau \in [3.45\,\text{ps}, 3.75\,\text{ps}]$.

experimental distribution. The interferograms of the incoherent ensembles differ significantly from each other, and they also differ qualitatively from the interferogram of the pure initial state. This simply reflects the fact that the dynamics of the $j = 2$ state is affected by more states in the initial ensemble. If one wants to test the composition of the initial state interferometrically, measurement of $j = 2$ is therefore preferred to $j = 0$. The visibility of the interferograms for $j = 2$ is reduced, compared to the pure state, to 0.85 for the experimental distribution of Ref. [14] and to 0.76 for the thermal state. These numbers are very encouraging in view of the feasibility of a rotational interferometer. In summary, incoherence in the initial state does not preclude interferometry, in particular if one measures the $j = 0$ population.

D. Prospect of measuring the polarizability anisotropy

The high visibility of the interferograms presented in Sec. III C suggests that the rotational interferometer can be employed to determine molecular parameters such as the polarizability anisotropy. Figure 7 shows interferograms obtained by measuring the final $j = 0$ population for several values of $\Delta\alpha$ – in atomic units: 16.20 a_0^3 (the *ab initio* value), 17.01 a_0^3 (5% larger) and 15.39 a_0^3 (5% smaller), increasing the peak intensity of the second pulse. Whereas the interferograms are essential identical for the three values of the polarizability anitropy if the pulses have the same intensity (Fig. 7a), the curves become more and more distinguishable when the intensity of the second pulse is increased (Fig. 7b-d). The better distinguishability comes at the price of a slightly deteriorated visibility of 0.79 for $I_0^2 = 1.6I_0^1$ (Fig. 7c) compared to 0.97 for equal intensities (Fig. 7a). Particularly promising features are observed for $I_0^2 = 1.6I_0^1$ in Fig. 7c for delays around 1.2 ps, 2.3 ps, 3 ps and 3.5 ps. Such clear differences should still be observable, even when inevitable error bars are taken into account.

Measurement errors in the final $j = 0$ population of 2% and 5% are assumed in Fig. 8(a) and (b), respectively. In the case of a 2% measurement error, the inter-

ferograms are easily distinguishable from each other, i.e., the curves including error bars do not overlap, in various ranges of time delays, for example for $\tau \in [1.5\,\mathrm{ps}, 2.0\,\mathrm{ps}]$, $[2.7\,\mathrm{ps}, 2.9\,\mathrm{ps}]$, or $[3.5\,\mathrm{ps}, 3.8\,\mathrm{ps}]$. For a 5% measurement error, however, only the latter interval of pulse delays allows to determine the polarizability anisotropy with a confidence level of ±5%. Within this region the interferogram is particularly sensitive to small variations in the molecular polarizability anisotropy. A zoom of this region is shown in Fig. 9, where two more values of $\Delta\alpha$, $16.52\,a_0^3$ and $15.88\,a_0^3$, larger by ±2% than the *ab initio* value, have also been included. It is seen that for a 2% measurement error the interferometer is readily sensitive to ±2% shifts in $\Delta\alpha$, whereas for a 5% measurement error, only shifts of ±5% can unequivocally be distinguished.

Our predictions for the sensitivity of the rotational interferometer are based on averaging over many wavepacket calculations to account for inevitable experimental inaccuracies. One might argue that the corresponding noise effects may come into play differently in the ERA and the full rovibrational dynamics. In order to be sure that our conclusions are not compromised by a break-down of the ERA, Figs. 8 and 9 compare the interferogram obtained within the ERA for the *ab initio* value of $\Delta\alpha$ with that obtained from full two-dimensional calculations, using Hamiltonian (1). While slight deviations in the error bars between ERA and 2D model are visible, in particular in Fig. 8(b) and 9(b), they are sufficiently small not to affect the confidence levels stated above. That is, a sensitivity of the interferometer to changes in the polarizability anisotropy of ±2% (±5%) requires the measurement errors not to exceed the same level.

IV. CONCLUSIONS

A Ramsey-type interferometer, employing off-resonant femtosecond laser pulses to induce rotational wavepacket dynamics in a trapped, cooled MgH^+ molecular ion, can be implemented using current experimental capabilities. Unlike in atom interferometry, where it is comparatively straight-forward to pick two isolated levels for Rabi cycling, application of the second pulse leads to rotational ladder climbing in the molecule. Perfect visibility of the interferogram can thus only be obtained for $j = 0$, whereas measuring $j = 2$ leads to 90%. It also requires a pure initial state with $j = 0$, $m = 0$.

Preparing a molecule perfectly in its rovibrational ground state is a very challenging task. However, a ground state population of 38%, as prepared in Ref. [14], is found to decrease the visibility for $j = 0$ to only 96% and that for $j = 2$ to only 85%. Even for a thermal distribution with a rotational temperature of 20 K, high-visibility interferograms are predicted. The required intensities are moderate for the case of the MgH^+ molecular ion, of the order of $10^{12}\,\mathrm{W/cm^2}$ for 100 fs laser pulses. This suggests feasibility of a rotational Ramsey interferometer, combining standard trapping and cooling techniques for molecular ions with 800 nm femtosecond laser pulses.

Such an interferometer could be used for example to determine the molecular polarizability anisotropy in the vibrational ground state by comparing an experimental interferogram to theoretical predictions for various values of $\langle\Delta\alpha\rangle_0$. Taking experimental uncertainties in the initial populations as well as population measurement errors into account, the interferometer is found to be sensitive to changes in the polarizability anisotropy of ±2%, respectively, ±5% assuming the same level of experimental inaccuracy.

It will be interesting to see whether the rotational Ramsey interferometer can also be used to determine the dependence of the molecular polarizability anisotropy on the internuclear separation. A possible route could be provided by recording rotational interferograms for several vibrational states. Alternatively, one could exploit the full rovibrational dynamics. In both cases, however, it might turn out to be difficult to disentangle effects that are due to the shape of the potential energy curve (which is also known only approximately) from those that are caused by the r-dependence of the polarizability anisotropy.

Additionally, the interferometric technique may be utilized to probe local electric fields, such as the radio-frequency fields at different positions within a (linear) Paul trap. Obviously, the rotational Ramsey interferometer will work as well for other molecular ion species, provided the laser light does not drive resonant transitions.

Acknowledgments

We would like to thank Rosario González-Férez and Daniel Reich for fruitful discussions. Financial support by the COST Action MP1001 IOTA, the Danish Ministry of Higher Education and Science through the Sapere Aude program and the European Commission under the Seventh Framework Programme FP7 GA 607491 COMIQ is gratefully acknowledged.

[1] P. R. Berman, ed., *Atom Interferometry* (Academic Press, 1997).
[2] N. F. Ramsey, *Molecular Beams* (Oxford University Press, 1956).
[3] R. Blatt and D. Wineland, Nature **453**, 1008 (2008).
[4] C. W. Chou, D. B. Hume, J. C. J. Koelemeij, D. J. Wineland, and T. Rosenband, Phys. Rev. Lett. **104**, 070802 (2010).

[5] P. F. Staanum, K. Højbjerre, R. Wester, and M. Drewsen, Phys. Rev. Lett. **100**, 243003 (2008).
[6] S. Haroche and J.-M. Raimond, *Exploring the Quantum* (Oxford Univ. Press, 2006).
[7] K. Højbjerre, A. K. Hansen, P. S. Skyt, P. F. Staanum, and M. Drewsen, New J. Phys. **11**, 055026 (2009).
[8] C. H. Townes and A. L. Schawlow, *Microwave Spectroscopy* (McGraw-Hill, New York, 1955).
[9] P. L. Jacobson, R. A. Komara, W. G. Sturrus, and S. R. Lundeen, Phys. Rev. A **62**, 012509 (2000).
[10] M. Aymar, R. Gurout, M. Sahlaoui, and O. Dulieu, J. Phys. B **42**, 154025 (2009).
[11] R. González-Férez and P. Schmelcher, New J. Phys. **11**, 055013 (2009).
[12] W. J. Balfour, Can. J. Phys. **50** (1972).
[13] A. K. Hansen, O. O. Versolato, L. Kłosowski, S. B. Kristensen, A. Gingell, M. Schwarz, A. Windberger, J. Ullrich, J. R. C. López-Urrutia, and M. Drewsen, Nature **508**, 76 (2014).
[14] P. F. Stanuum, K. Højbjerre, P. S. Skyt, A. K. Hansen, and M. Drewsen, Nature Physics **6**, 271 (2010).